

El Niño–Southern Oscillation Sea Level Pressure Anomalies in the Western Pacific: Why Are They There?*

XUAN JI, J. DAVID NEELIN, AND C. ROBERTO MECHOSO

Department of Atmospheric and Oceanic Sciences, University of California, Los Angeles, Los Angeles, California

(Manuscript received 22 October 2014, in final form 17 June 2015)

ABSTRACT


Although sea level pressure (SLP) anomalies in the western Pacific have long been recognized as an integral part of the classic Southern Oscillation pattern associated with El Niño–Southern Oscillation (ENSO), there is an unresolved question regarding the dynamics that maintain these anomalies. Traditional studies of the ENSO response in the tropics assume a single deep baroclinic mode associated with the tropospheric temperature anomalies. However, the SLP anomalies in the western Pacific are spatially separated from the baroclinic signal in the NCEP–NCAR reanalysis, CMIP5 models, and an intermediate complexity model [a quasi-equilibrium tropical circulation model (QTCM)]. Separation of ENSO SLP anomalies in the tropical Pacific into baroclinic and barotropic components indicates that the barotropic component contributes throughout the tropics and constitutes the primary contribution in the western Pacific. To demonstrate the roles of baroclinic and barotropic modes in ENSO teleconnections within the tropics, a series of QTCM experiments is performed, where anomalies in the interactions between baroclinic and barotropic modes are suppressed over increasingly wider latitudinal bands in the tropical Pacific. If this suppression is done in the 15°N–15°S band, the pressure signals in the western Pacific are only partly removed, whereas if it is done in the 30°N–30°S band, the anomalies in the western Pacific are almost entirely removed. This suggests the following pathway: interactions with SST anomalies create the baroclinic response in the central and eastern Pacific, but baroclinic–barotropic interactions, arising substantially in the subtropical Pacific, generate a barotropic response that yields the SLP anomalies in the western Pacific.

1. Introduction

El Niño–Southern Oscillation (ENSO) is associated with sea level pressure (SLP) anomalies that have long been recognized to form an oscillation pattern with poles in the western equatorial and southeastern Pacific (e.g., Walker 1923; Berlage 1957; Wallace et al. 1998). ENSO is also associated with tropospheric temperature anomalies that spread from the central and eastern Pacific and that

in many ways resemble basic equatorial wave dynamics (Kiladis and Diaz 1989; Wallace et al. 1998; Chiang and Sobel 2002; Su and Neelin 2002; Kumar and Hoerling 2003). Some major aspects of ENSO dynamics can be understood through conceptual models based on a single deep baroclinic mode that is separable from the barotropic mode in the absence of baroclinic advection and vertical turbulent momentum transport (Matsuno 1966; Webster 1972; Gill 1980). Such highly damped shallow-water models often give a plausible first approximation to the low-level wind response in the immediate vicinity of ENSO convective heating anomalies.

As we will show in the analysis in section 3, motivated by results from Wallace et al. (1998), the SLP anomalies in the western tropical Pacific are spatially separated from the baroclinic signal associated with the tropospheric temperature anomalies over the central and eastern Pacific. This raises a puzzle: if there are no significant ENSO-associated tropospheric temperature anomalies in the western Pacific, then the SLP anomaly

 Denotes Open Access content.

* Supplemental information related to this paper is available at the Journals Online website: <http://dx.doi.org/10.1175/JCLI-D-14-00716.s1>.

Corresponding author address: J. David Neelin, Department of Atmospheric and Oceanic Sciences, UCLA, 7127 Math Sciences Building, 405 Hilgard Ave., Los Angeles, CA 90095-1565.
E-mail: neelin@atmos.ucla.edu

DOI: 10.1175/JCLI-D-14-00716.1

cannot be due to a baroclinic response in that region. In other words, a conceptual model including only a baroclinic mode cannot explain the western Pacific portion of the canonical ENSO SLP anomaly.

Teleconnections from the ENSO heating region into the midlatitudes are largely barotropic (Horel and Wallace 1981; Hoskins and Karoly 1981; Simmons 1982; Branstator 1983; Simmons et al. 1983; Held and Kang 1987) because the barotropic mode can reach high turning latitudes. Lee et al. (2009) have analyzed the interaction of baroclinic and barotropic components in the response to ENSO-like heating, as well as the importance of vertical background wind shear in exciting the barotropic response in midlatitudes. In intermediate complexity models in which both barotropic and baroclinic components are included, such as the quasi-equilibrium tropical circulation model (QTCM) used in part of this study (Neelin and Zeng 2000, hereinafter NZ00; Zeng et al. 2000), the barotropic component forms an important part of the solution in climatology and ENSO variations. It is thus natural to ask whether the resolution to the above-mentioned puzzle might lie in the barotropic component of the ENSO response within the tropics, which appears so far not to have been extensively examined.

In the present study we show that in reanalysis data the western Pacific SLP response is part of a widespread barotropic contribution to the ENSO signal, whose spatial pattern differs substantially from the baroclinic signal. We then turn to model analysis and mechanism suppression experiments to argue that within the tropics, barotropic teleconnections excited by the baroclinic–barotropic interactions are responsible for the ENSO atmospheric response in SLP over the tropical western Pacific. Our hypothesis is the following: as baroclinic Rossby waves propagate west from the central and eastern equatorial Pacific, they excite barotropic wave trains through barotropic–baroclinic interactions. These wave trains can then propagate west to generate the SLP anomalies in the western Pacific, where it is observed that the baroclinic mode propagation does not reach. The barotropic mode can be forced by three barotropic–baroclinic interaction terms: 1) shear advection (Wang and Xie 1996; Majda and Biello 2003; Biello and Majda 2004b), 2) surface drag (NZ00; Biello and Majda 2004a), and 3) vertical advection (Bacmeister and Suarez 2002). Recently, Ji et al. (2014) provided a detailed analysis of the effects these three terms have in interhemispheric teleconnections from tropical heat sources.

To demonstrate the respective roles of baroclinic and barotropic modes in ENSO teleconnections within the tropics, we first analyze the teleconnection patterns in the NCEP reanalysis and in several simulations done with general circulation models (GCMs) participating in phase 5 of the Coupled Model Intercomparison Project

(CMIP5). Then to analyze the dynamics that maintain the SLP anomalies in the western Pacific associated with ENSO, we perform a set of diagnostic experiments using the QTCM, where the impact of the baroclinic–barotropic interaction terms on the SLP anomalies in the western Pacific can be artificially suppressed.

The remainder of the text is organized as follows: Section 2 gives a brief introduction of the datasets, model, and methodology used in this study. Section 3 presents the analysis of baroclinic and barotropic modes in ENSO tropical teleconnections, based on data from the NCEP–NCAR reanalysis and CMIP5 simulations. Section 4 presents the results of several diagnostic experiments with the QTCM that demonstrate the dynamical pathway involved in ENSO tropical teleconnections. Section 5 consists of a summary and a discussion.

2. Datasets, model, and methodology

a. Datasets

We use monthly diagnostic surface temperature from NOAA NCEP–NCAR Climate Data Assimilation System 1 (CDAS-1; <http://iridl.ldeo.columbia.edu/SOURCES/NOAA/NCEP-NCAR/CDAS-1/MONTHLY/Diagnostic/surface/temp/?Set-Language=en>; Kalnay et al. 1996) to compute the Niño-3.4 SST index (Trenberth 1997). Meteorological variables including sea level pressure, air temperature, sea surface temperature, and precipitation are taken from NCEP–NCAR reanalysis (<http://www.esrl.noaa.gov/psd/data/gridded/data.ncep.reanalysis.html>; Kalnay et al. 1996) and AMIP runs using prescribed SST anomalies for the period 1980–2008 of several models participating in CMIP5 (http://cmip-pcmdi.llnl.gov/cmip5/cmip5_references.html; Taylor et al. 2012). For presentation, we only show results from four atmospheric general circulation models (AGCMs): CCSM4, CanAM4, GISS, and GFDL HiRAM-C360.

b. Conditions of baroclinic and barotropic mode separation

In this subsection we summarize conditions of separation of baroclinic and barotropic modes, and the methods and approximations involved in computing barotropic and baroclinic components of SLP in both reanalysis data and AGCM outputs.

The hydrostatic equation in pressure coordinates, $\partial_p \phi = -RT/p$, can be expressed in vertical integral form as

$$\phi = \int_p^{p_r} RT d \ln p + \phi_r, \quad (1)$$

where ϕ is the geopotential at pressure level p , T is temperature, R is the gas constant for air, p_r is a reference

pressure, and ϕ_r is the geopotential on that pressure surface. The momentum equation of the primitive equations combined with the hydrostatic equation can be written as

$$\begin{aligned} (\partial_t + \mathbf{v} \cdot \nabla + \omega \partial_p - K_H \nabla^2) \mathbf{v} + f \mathbf{k} \times \mathbf{v} + g \partial_p \tau \\ = -\nabla \int_p^{p_r} RT d \ln p - \nabla \phi_r, \end{aligned} \quad (2)$$

where \mathbf{v} is horizontal velocity, ω is vertical velocity in pressure coordinates, K_H is the horizontal diffusion coefficient, f is the Coriolis parameter, τ is the vertical flux of horizontal momentum, and g is gravitational acceleration. Separation of the baroclinic and barotropic modes occurs under the following conditions: neglecting advection by baroclinic velocity (horizontal and vertical components) and neglecting the contribution of baroclinic wind in the surface drag on the barotropic mode. Under these circumstances the solution of Eq. (2) for velocity must simply match the vertical structures of the barotropic and baroclinic pressure gradient terms. The barotropic mode has constant vertical structure, since by definition it has no contribution from temperature yielding vertical variations in Eq. (2). These conditions are typically not met in subtropical to midlatitude conditions (e.g., Held et al. 1985), but it has been common to assume separation for simple tropical models such as Gill (1980). We argue here that the baroclinic–barotropic interactions cannot be neglected for important aspects of the tropical solutions. In diagnosing this, it is useful to compute components of the flow associated with the barotropic and baroclinic contributions. We underline, however, that these should not be viewed as perfectly separated modes—the interaction terms will be introduced in the next section for the case where a deep baroclinic component and the barotropic component are the leading contributors to the solution.

Because the barotropic pressure gradient has no vertical variation and the velocity component matches this vertical structure, a vertical average can be used to diagnose the barotropic contribution (projections on this decomposition are further discussed in the next section). The vertical average over the troposphere is $\hat{X} = \langle X \rangle = p_T^{-1} \int_{p_r}^{p_{rs}} X dp$, where p_{rs} and p_{rt} are pressure at the near-surface and tropopause reference levels, respectively (here, 1000 and 150 hPa, respectively); and $p_T = p_{rs} - p_{rt}$. The barotropic component of the geopotential can be defined as $\phi_0 = \langle \phi \rangle$ for all levels. The barotropic (subscript 0) and baroclinic (subscript 1) components of the near-surface (1000 hPa) geopotential are thus defined by

$$\phi_{rs0} = \langle \phi \rangle, \quad \text{and} \quad \phi_{rs1} = \phi_{rs} - \phi_{rs0}, \quad (3)$$

that is, $\phi_{rs} = \phi_{rs0} + \phi_{rs1}$. Working in pressure coordinates, this near-surface geopotential contains the

key dynamical information, but since sea level pressure is the traditional diagnostic, we present figures here in terms of sea level pressure. Furthermore, we are interested in departures from long-term time averages (\prime). Assuming that density ρ_s is constant between the surface and the near-surface reference levels, and using Eq. (3) with ϕ obtained directly from the reanalysis and model outputs, the baroclinic and barotropic components of the surface pressure perturbations are then

$$p'_s \approx \rho_s \phi'_{rs0} + \rho_s \phi'_{rs1}. \quad (4)$$

A second way to do the decomposition is to compute ϕ from temperature via Eq. (1), and then calculate

$$p'_{s1} = \rho_s (\phi'_s - \langle \phi' \rangle), \quad \text{and} \quad p'_{s0} = p'_s - p'_{s1}, \quad (5)$$

where surface pressure p_s is obtained directly from the reanalysis and model outputs. The first choice [Eq. (4)] benefits from all computations having been done at the model native levels, while the second method [Eq. (5)] has the advantage of permitting computation of temperature perturbations through different layers (in particular, boundary layer vs free troposphere). Results from both computations are compared in Figs. S1 and S2 (see the supplemental material), further discussed below, and are in good agreement for all major features. The calculations in Eq. (5) are used in reanalysis and model figures in the main text.

c. Baroclinic and barotropic mode interactions in the QTCM

The QTCM belongs to a class of tropical atmospheric models of intermediate complexity that occupies a niche between GCMs and simple models. The model takes analytical solutions that hold approximately under quasi-equilibrium (QE) conditions and employs them as leading basis functions to represent the vertical structure of the flow. The primitive equations are then projected onto these simplified vertical structures, with self-consistent nonlinear terms retained in advection, moist convection, and vertical momentum transfer terms, among others. A more detailed model description can be found in NZ00.

The QTCM has been used to analyze the moist dynamics of ENSO teleconnections in a number of contexts (Su et al. 2001, 2003, 2005; Neelin and Su 2005; Lintner and Chiang 2007). The present study uses the first-generation QTCM (QTCM1), version 2.3, which retains a single basis function for the vertical structure of temperature, with two components [barotropic V_0 and baroclinic $V_1(p)$] in the vertical structure of velocity. This is the simplest configuration, but it has considerable success in capturing tropical phenomena because the

temperature structure matches the consequences of a quasi-equilibrium convective scheme and the baroclinic velocity basis function is analytically compatible. Thus, the QTCM provides an appealing tool to analyze the contributions of baroclinic and barotropic modes to the ENSO tropical teleconnections. We note here that the subscript 1 in this section refers to the single deep baroclinic mode in the QTCM, which is a little different from the notation in the previous section, where subscript 1 refers to the baroclinic contribution that can have any vertical structure.

In the QTCM, the momentum Eq. (2) is projected onto the barotropic and baroclinic wind components $\mathbf{v}_0(x, y, t)$ and $\mathbf{v}_1(x, y, t)$, respectively. For the barotropic component:

$$\partial_t \mathbf{v}'_0 + D_{V_0}(\mathbf{v}_0, \mathbf{v}_1)' + f\mathbf{k} \times \mathbf{v}'_0 + (g/p_T)\tau'_s = -\nabla \phi'_{s0} \quad (6)$$

with

$$D_{V_0}(\mathbf{v}_0, \mathbf{v}_1)' = (\mathbf{v}_0 \cdot \nabla \mathbf{v}_0)' + (\langle V_1^2 \rangle \mathbf{v}_1 \cdot \nabla \mathbf{v}_1)' + [\langle V_1^2 \rangle (\nabla \cdot \mathbf{v}_1) \mathbf{v}_1]' - K_H \nabla^2 \mathbf{v}'_0, \quad (7)$$

where $V_1(p)$ is the vertical structure of the baroclinic component. The baroclinic wind component is governed by

$$\partial_t \mathbf{v}'_1 + D_{V_1}(\mathbf{v}_0, \mathbf{v}_1)' + f\mathbf{k} \times \mathbf{v}'_1 + g \langle V_1^2 \rangle^{-1} \langle V_1 \partial_p \tau \rangle' = -\kappa \nabla T'_1, \quad (8)$$

where $D_{V_1}(\mathbf{v}_0, \mathbf{v}_1)'$ is the advection–diffusion operator similar to Eq. (7) but for the baroclinic wind component. The geopotential gradient term $\kappa \nabla T'_1$ appears simple because $V_1(p)$ has been chosen to match the hydrostatic integral of the vertical structure of temperature, $a_1(p)$, with $\kappa = R/c_p$, where c_p is the heat capacity of air at constant pressure. The temperature coefficient, $T_1(x, y, t)$, is governed by the temperature equation for deep baroclinic structure:

$$\langle a_1 \rangle (\partial_t + D_{T_1}) T_1 + M_{S_1} \nabla \cdot \mathbf{v}_1 = \langle Q_c \rangle + \langle Q_R \rangle, \quad (9)$$

where D_{T_1} is the advection–diffusion operator for temperature; M_{S_1} is the dry static stability for a vertical velocity profile derived from $V_1(p)$; and $\langle Q_c \rangle$ and $\langle Q_R \rangle$ are the vertical average convective and radiative plus sensible heating of the column, respectively. The convective heating is given by the convective parameterization that depends on temperature and moisture, with the moisture equation vertically projected on a single basis function (see NZ00 for details and other definitions). The driving by SST appears in the surface radiative and sensible heat fluxes that contribute to $\langle Q_R \rangle$ and in

evaporation, as in a standard primitive equation model. The SST thus directly forces a prognostic baroclinic response in temperature, moisture, and baroclinic wind. The barotropic response is forced by the baroclinic response through the interaction terms in Eq. (6), including surface drag and the baroclinic advection terms given by Eq. (7).

In diagnosing near-surface geopotential perturbation, the baroclinic contribution ϕ'_{s1} is obtained analytically from the vertical structure of temperature using the hydrostatic equation (as in NZ00):

$$\phi'_{s1} = -R \left\langle \int_p^{p_s} a_1(p) d \ln p \right\rangle T'_1 \quad (10)$$

and the barotropic contribution ϕ'_{s0} is calculated from Eq. (6). The total surface pressure p'_s is then diagnosed with $p'_s = \rho_s \phi'_{s1} + \rho_s \phi'_{s0}$ as in Eq. (4).

Taking the curl_z of Eq. (6), the equation for the barotropic streamfunction ψ_0 is

$$\begin{aligned} \partial_t \nabla^2 \psi'_0 + \text{curl}_z(\mathbf{v}_0 \cdot \nabla \mathbf{v}_0)' - K_H \nabla^4 \psi'_0 + \beta \mathbf{v}'_0 \\ = -\text{curl}_z(\langle V_1^2 \rangle \mathbf{v}_1 \cdot \nabla \mathbf{v}_1)' - \text{curl}_z[\langle V_1^2 \rangle (\nabla \cdot \mathbf{v}_1) \mathbf{v}_1]' \\ - \text{curl}_z(\varepsilon_0 \mathbf{v}_0 + \varepsilon_{10} \mathbf{v}_1)', \end{aligned} \quad (11)$$

where β is the meridional derivative of the Coriolis parameter, $(g/p_T)\tau'_s$ is parameterized with $(\varepsilon_0 \mathbf{v}_0 + \varepsilon_{10} \mathbf{v}_1)'$, and where ε_0 and ε_{10} are momentum transfer rates from projection of turbulent stress terms as in NZ00. The terms on the right-hand side of Eq. (11) act as an effective Rossby wave source (RWS), which acts to excite the barotropic mode in a manner akin to well-known studies of barotropic teleconnections (Hoskins and Karoly 1981; Held and Kang 1987; Sardeshmukh and Hoskins 1988). We remark, first, that this is not quite the same as the Rossby wave source that would be defined by assuming an upper-level forcing applied to the barotropic mode, but rather results from a representation of the modal breakdown over the full depth of the troposphere (NZ00; Majda and Biello 2003). Under certain circumstances, in particular if one could assume horizontally constant vertical shear in the geostrophic approximation, an alternate vertical mode decomposition can be constructed in which the barotropic mode properties are modified to create an external or equivalent barotropic mode with some baroclinic component included (Held et al. 1985). The interaction term approach here treats the same process in a manner that is easier to use in a spatially varying basic state. Second, the third term on the right-hand side is shown in a form where it is proportional to surface stress, which can be simpler for diagnosis and interpretation. However, it might alternately be separated into a forcing term $-\text{curl}_z(\varepsilon_{10} \mathbf{v}_1)'$, with the $-\text{curl}_z(\varepsilon_0 \mathbf{v}_0)'$ portion on the left-hand side.

NCEP NINO3.4 Regression DJF 1982-2008

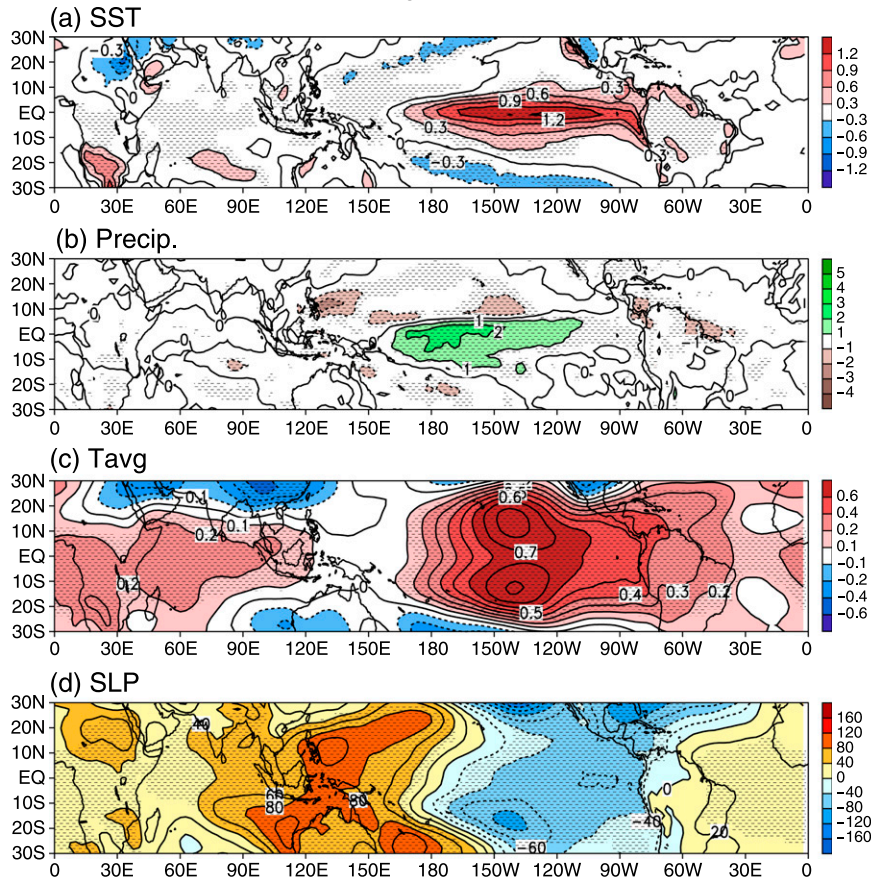


FIG. 1. (a) SST ($\text{K } ^\circ\text{C}^{-1}$), (b) precipitation ($\text{mm day}^{-1} \text{ } ^\circ\text{C}^{-1}$), (c) tropospheric temperature ($\text{K } ^\circ\text{C}^{-1}$), and (d) SLP ($\text{Pa } ^\circ\text{C}^{-1}$) from NCEP–NCAR reanalysis DJF regression onto Niño-3.4, with a two-tailed t test applied to the regression values and stippled at 99% confidence.

Interpreting the respective terms in the effective Rossby wave source in Eq. (11), the sources of baroclinic–barotropic interaction are 1) $-\text{curl}_z(\langle V_1^2 \rangle \mathbf{v}_1 \cdot \nabla \mathbf{v}_1)'$, representing interactions of vertical shear in horizontal advection terms; 2) $-\text{curl}_z[\langle V_1^2 \rangle (\nabla \cdot \mathbf{v}_1) \mathbf{v}_1]'$, representing vertical motion advecting the baroclinic wind component; and 3) $-\text{curl}_z(\varepsilon_0 \mathbf{v}_0 + \varepsilon_{10} \mathbf{v}_1)'$, representing interactions via surface stress in the boundary layer. Ji et al. (2014) analyzed the effects of each mechanism on the forcing of the barotropic mode and associated teleconnection pathways from a tropical heat source.

We perform several diagnosis experiments with the QTCM to analyze the pathway for the atmospheric response in the tropical western Pacific associated with ENSO. In these experiments, the interannual variations in the baroclinic–barotropic interaction terms are suppressed by replacing these terms with their monthly mean values from a 100-yr climatological model run. To gain insight on the geographical extent of the region where the interactions act in the

tropical teleconnections, interannual variations are suppressed over increasingly wider latitudinal bands in the tropical Pacific.

3. Baroclinic and barotropic modes in ENSO tropical teleconnections

In this section we examine the meteorological anomalies associated with ENSO. These are defined by regression of each quantity onto the Niño-3.4 SST index. We start with the monthly means for the winter season [December–February (DJF)] in the NCEP–NCAR reanalysis. The results, shown in the panels of Fig. 1, are in good agreement with previous observational results, notably from Wallace et al. (1998), a study that helped inspire the investigation here.

In Fig. 1a, the SST anomalies show positive values in the central and eastern equatorial Pacific. Figure 1b shows positive precipitation anomalies around the central equatorial Pacific with negative anomalies around

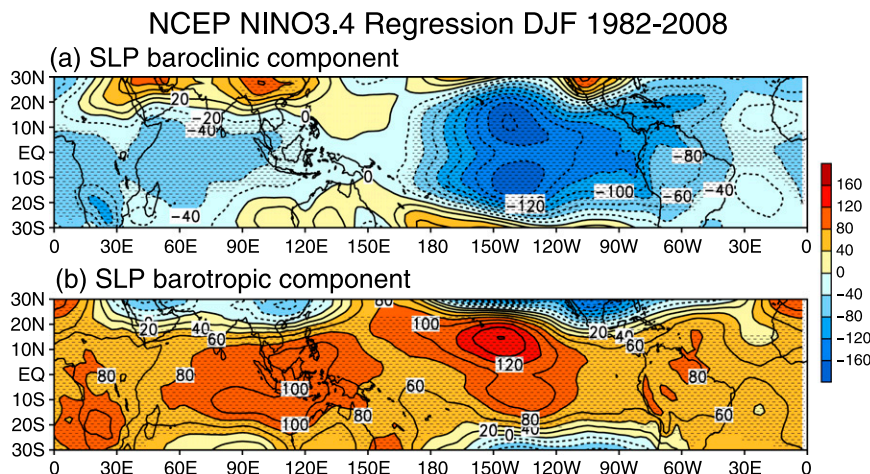


FIG. 2. (a) SLP baroclinic component ($\text{Pa } ^\circ\text{C}^{-1}$) and (b) SLP barotropic component ($\text{Pa } ^\circ\text{C}^{-1}$) from NCEP–NCAR reanalysis DJF regression onto Niño-3.4, with a two-tailed t test applied to the regression values and stippled at 99% confidence.

them and maximum values slightly to the west of the largest SST anomalies. The anomalies in vertical mean tropospheric temperature (Fig. 1c) show positive values over a broad region of the tropical central and eastern Pacific. The structure of these temperature anomalies is consistent with a baroclinic Rossby wave straddling the equator to the west and a Kelvin wave around the equator to the east of the precipitation anomalies in Fig. 1b, which correspond to regions of deep convective heating anomalies. The magnitude of the tropospheric temperature anomalies drops off sharply from around the date line toward the western Pacific. The lack of baroclinic mode propagation toward the west is at least in part due to the slow phase speed of baroclinic Rossby wave packets, although it may also be affected by more complex factors, such as the slower speed of waves interacting strongly with convection. In either case, it is clear that the deep baroclinic anomalies do not reach the western Pacific. The SLP anomalies (Fig. 1d) are reminiscent of the classic Southern Oscillation pattern: strong negative and positive anomalies in the eastern and western Pacific, respectively. Thus, in the western Pacific the SLP anomalies are spatially separated from the baroclinic signal associated with the temperature anomalies.

Next, we break down the SLP anomalies in Fig. 1d into their baroclinic and barotropic components. The baroclinic component (Fig. 2a) has strong magnitudes in the eastern Pacific in the same region where tropospheric temperature anomalies are strong (Fig. 1c), as expected from the hydrostatic relationship. The barotropic component (Fig. 2b), on the other hand, shows a broad band of anomalies across the entire tropics with a clear local maximum in the western Pacific, where the

values are comparable to those of the total SLP anomalies in Fig. 1d. Thus, the positive SLP anomalies in the western Pacific are due to the barotropic contribution, since the baroclinic contribution has the opposite sign and is small.

The robustness of the results in Figs. 1 and 2 is examined in several figures in the supplemental material. Similar results are obtained for regression of monthly anomalies over the full annual cycle (Fig. S1 in the supplemental material) and using Eq. (4) instead of Eq. (5) to decompose the SLP anomalies into baroclinic and barotropic components (Fig. S2 in the supplemental material). The conclusion in Fig. 2 that the barotropic contribution is not negligible even in the deep tropics also holds when viewed in terms of the associated surface wind contributions (Figs. S3 and S4 in the supplemental material). In the subtropics, the barotropic wind contribution considerably cancels the baroclinic contribution to the surface wind, as one would expect when surface drag is effective at damping the near-surface baroclinic wind component and spinning up a barotropic wind component. Finally, the baroclinic contribution to SLP anomalies in Fig. 2a comes primarily from the free troposphere rather than the boundary layer (Fig. S5 in the supplemental material). In either case, baroclinic contributions to SLP anomalies in the western Pacific are very weak.

In the following, we examine the anomalies in SLP and tropospheric temperature associated with ENSO in the AGCM simulations described in section 2 using the monthly mean fields for the winter season. We show in Fig. 3 the SLP and the tropospheric temperature anomalies based on models participating in the CMIP5. Thirty models are examined but four typical models are shown, which are consistent at large scales with the corresponding patterns in the NCEP–NCAR reanalysis

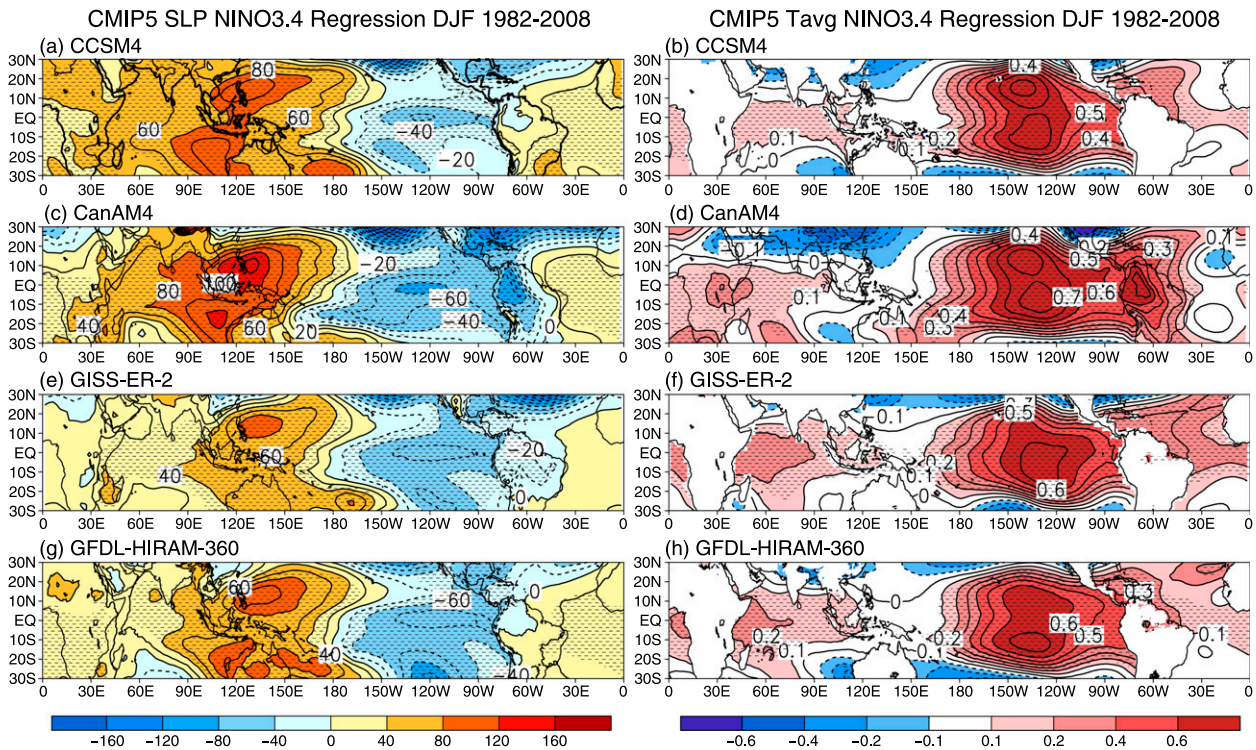


FIG. 3. (left) SLP ($\text{Pa } ^\circ\text{C}^{-1}$) and (right) tropospheric temperature ($\text{K } ^\circ\text{C}^{-1}$) from selected AGCM runs participating in CMIP5 DJF regression onto Niño-3.4, with a two-tailed t test applied to the regression values and stippled at 99% confidence.

(Fig. 1). The large SLP anomalies and weak tropospheric temperature anomalies in the western Pacific are also present in the AGCMs of other CMIP5 models (not shown). When model SLP anomalies are decomposed into baroclinic and barotropic components (Fig. S6 in the supplemental material), the barotropic contribution dominates in the western Pacific, where the baroclinic contribution is small as in the NCEP–NCAR reanalysis (Fig. 2). Examining the model SLP patterns in Figs. 3a, 3c, 3e, and 3g in more detail, some variation may be noted in the western Pacific, suggesting that while the overall mechanism is common among the models, there may be some sensitivity in the precise spatial pattern and amplitude.

In section 4, the dynamical mechanisms at work in the ENSO tropical teleconnection process are investigated using QTCM. First, it is necessary to confirm the extent to which the QTCM has a similar response to ENSO as in the NCEP–NCAR reanalysis and CMIP5 models. Figure 4 shows the wintertime meteorological anomalies associated with ENSO based on the 26 winters (DJF) in a 27-yr (1982–2008) QTCM run with observed SSTs. A comparison between panels in Fig. 4 with those obtained using the NCEP–NCAR reanalysis in Figs. 1 and 2 reveals similarities of pattern, although simulated amplitudes are weaker. This is possibly due to the simplified vertical structure of temperature in the QTCM, which

tends to cause the tropospheric temperature anomalies to be more strongly damped toward SST anomalies. For the purpose of this study, the similarities of pattern between the QTCM and reanalysis data are sufficient to motivate analysis of mechanisms in a model where the baroclinic–barotropic interaction terms can be explicitly altered.

4. Diagnosis experiment with the QTCM

In this section, we use the QTCM to gain insight into the dynamical mechanisms at work for the ENSO tropical teleconnection process. The question to be addressed is how the barotropic teleconnection patterns are forced in the western Pacific by the effective barotropic Rossby wave source due to the baroclinic–barotropic interactions. This is examined by conducting mechanism-suppression experiments in which anomalies in the baroclinic–barotropic interaction terms are artificially suppressed over specified regions. The results in this section are based on pairs of 100-yr QTCM simulations: one with monthly composites of El Niño SST anomalies added to monthly mean climatology (El Niño run) and the other with monthly mean climatological SSTs (climatological run). The El Niño run monthly SST anomalies are composited from July through the following June of five large El Niño events

QTCM NINO3.4 Regression DJF 1982-2008

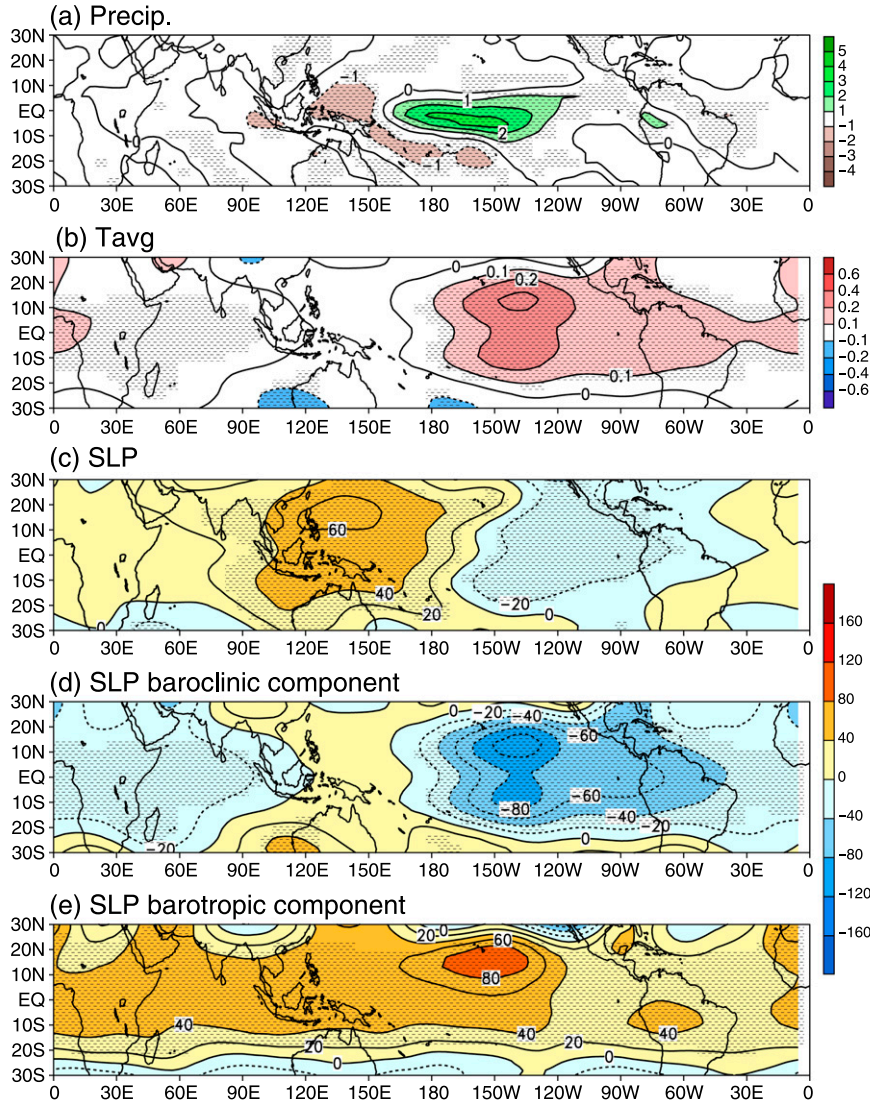


FIG. 4. (a) Precipitation ($\text{mm day}^{-1} \text{ } ^\circ\text{C}^{-1}$), (b) tropospheric temperature ($\text{K } ^\circ\text{C}^{-1}$), (c) SLP ($\text{Pa } ^\circ\text{C}^{-1}$), (d) SLP baroclinic component ($\text{Pa } ^\circ\text{C}^{-1}$), and (e) SLP barotropic component ($\text{Pa } ^\circ\text{C}^{-1}$) from a 27-yr (1982–2008) QTCM run with real-time SSTs DJF regression onto Niño-3.4, with a two-tailed t test applied to the regression values and stippled at 99% confidence.

(1957/58, 1965/66, 1972/73, 1982/83, and 1997/98). The 100-yr simulation length is used to obtain statistically significant results, including in the western Pacific when the signal is artificially reduced. The barotropic–baroclinic interaction terms for the QTCM barotropic Eq. (11) are saved from the climatological run, and are specified as a seasonally varying source term in the specified target region of the suppression experiments. Each pair of El Niño and climatological runs is conducted with the same climatological barotropic–baroclinic interaction terms specified in the target region. Differences between each pair are thus due to the response to SST

anomalies in the absence of barotropic–baroclinic interaction term anomalies within the target region.

Figure 5 shows the December–February mean SST anomalies, precipitation anomalies, tropospheric average temperature anomalies, SLP anomalies, and the baroclinic and barotropic SLP anomalies (differences) between the El Niño run and the climatological run with full Rossby wave source (i.e., no suppression). Each panel shows a similar pattern to the one obtained by regressing each variable onto Niño-3.4 SST shown in Figs. 1 and 2 for NCEP reanalysis data and Fig. 4 from a 27-yr (1982–2008) QTCM run with observed SSTs. Note

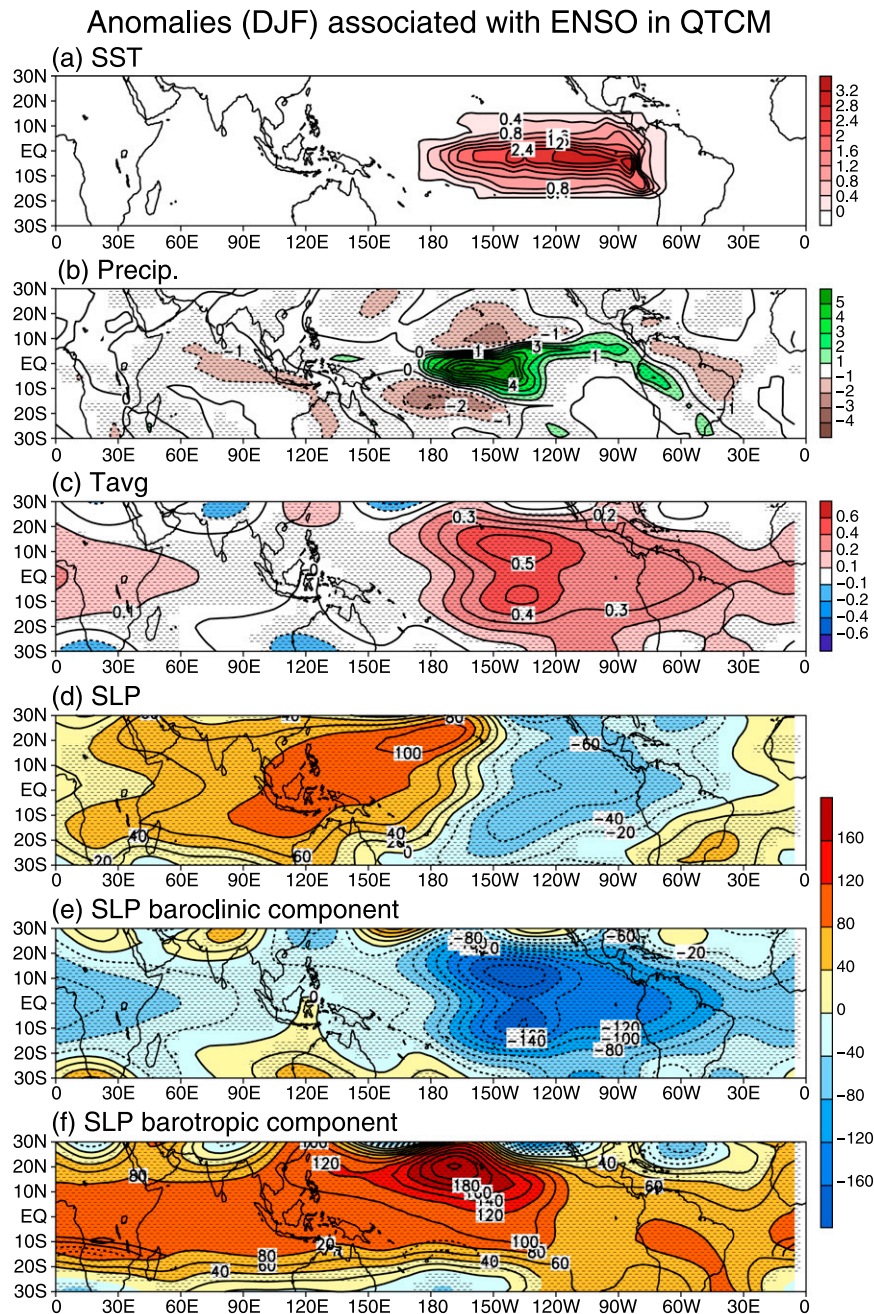


FIG. 5. (a) SST anomaly ($^{\circ}\text{C}$), (b) precipitation anomaly (mm day^{-1}), (c) tropospheric temperature anomaly (K), (d) SLP anomaly (Pa), (e) SLP anomaly baroclinic component (Pa), and (f) SLP anomaly barotropic component (Pa) associated with ENSO from the QTCM experiment with full barotropic RWS (i.e., no suppression), stippled where a t test yields grid points significant at or above the 99% confidence level.

that the regression plots in Fig. 4 show values per degree of SST anomalies associated with ENSO, whereas the fields in Fig. 5 are associated with SST anomalies on the order of 2–3 K (Fig. 5a). Thus, values in Fig. 5 are all 2–3 times larger than those in Fig. 4. The breakdown of the

SLP anomalies (Fig. 5d) into the baroclinic (Fig. 5e) and barotropic (Fig. 5f) components again indicates that the positive SLP anomalies in the western Pacific, especially the maximum around 180° , 20°N , are due to the barotropic contribution.

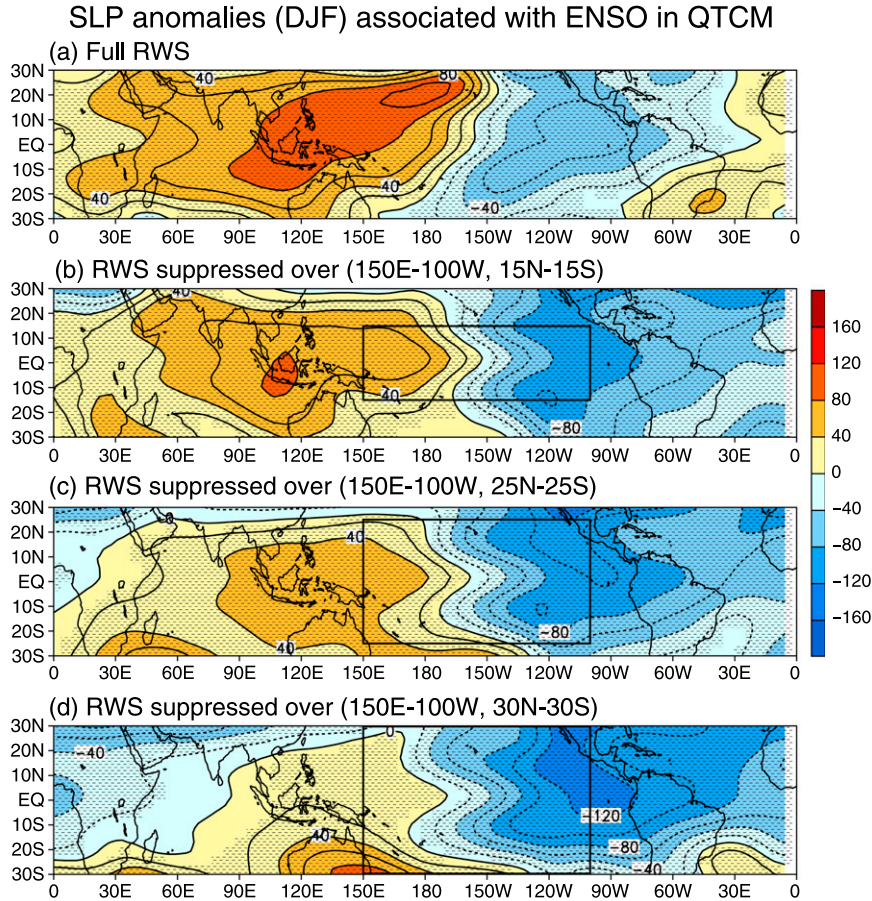


FIG. 6. SLP anomaly (Pa) associated with ENSO from QTCM experiments with (a) full barotropic RWS; (b) RWS suppressed over 15°N–15°S, 150°E–100°W; (c) RWS suppressed over 25°N–25°S, 150°E–100°W; and (d) RWS suppressed over 30°N–30°S, 150°E–100°W, stippled as in Fig. 5. Box indicates the region of RWS suppression.

Figure 6 displays the December–February mean SLP differences between the El Niño run and the climatological run. The SLP anomalies in Fig. 5d are repeated in Fig. 6a. Figures 6b–d portray the impact of suppressing the Rossby wave source anomalies in the region from 150°E to 100°W for successively wider latitudinal bands around the equator. Comparisons among Figs. 6b–d reveal that the SLP anomalies in the western Pacific are gradually weaker with wider bands of suppression. This weakening indicates that the baroclinic–barotropic interactions in the Pacific subtropics are important in addition to those in the tropics to the SLP anomalies in the western Pacific.

Figure 7 presents the total Rossby wave source (Fig. 7a) as well as its three components (shear advection, surface drag, and vertical advection) between the two 100-yr simulations, that is, the Rossby wave source that we suppressed in the QTCM experiments in Fig. 6. The surface drag (Fig. 7c) and vertical advection

(Fig. 7d) terms each have nonnegligible contributions in the equatorial central Pacific. Note that Fig. 7c shows the baroclinic portion $-\text{curl}_z(\epsilon_{10}\mathbf{v}_1)'$ as the forcing component in the surface drag, since the barotropic portion $-\text{curl}_z(\epsilon_0\mathbf{v}_0)'$ acts as damping on the barotropic mode, while in the QTCM experiment we suppress the surface stress term as a whole. The shear advection term (Fig. 7b) tends to have the largest contribution, especially in the subtropics. This horizontal advection term arises substantially from the baroclinic wind anomalies interacting with basic-state vertical shear. The importance of the horizontal shear advection term in the subtropics is consistent with the need to suppress the Rossby wave source through the latitude band that includes the subtropics in the suppression experiments to reduce barotropic signal in the western Pacific. The strong subtropical horizontal shear contribution results when the ENSO baroclinic anomaly spreads in latitude over roughly an equatorial radius of deformation, as was

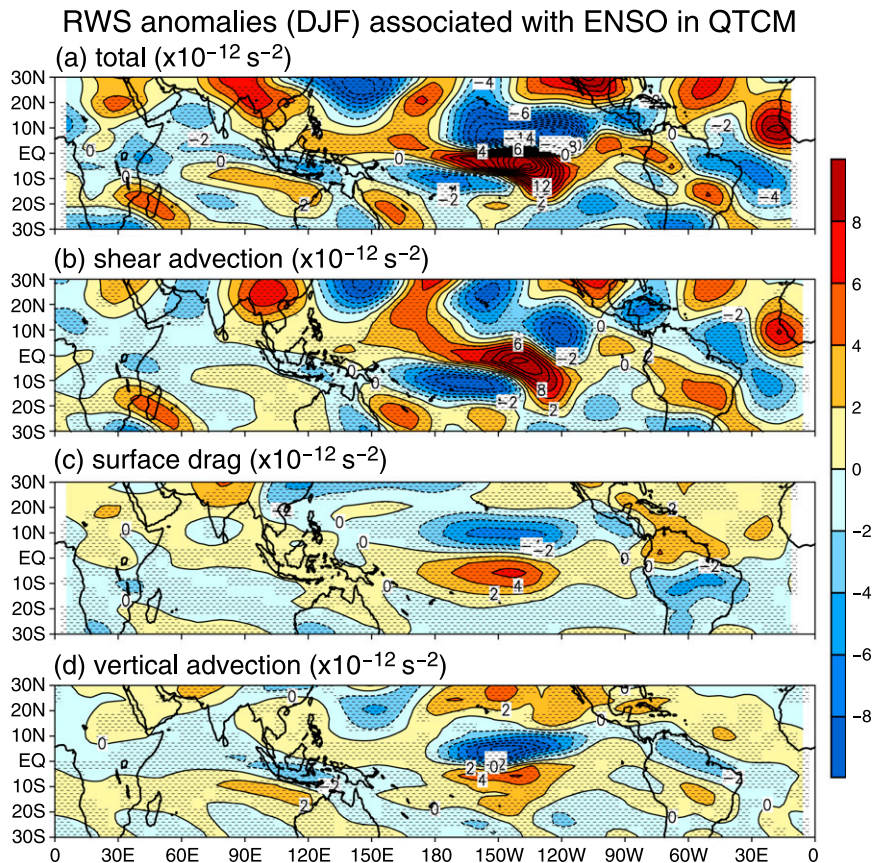


FIG. 7. QTCM barotropic RWS anomalies associated with ENSO. (a) Total, (b) shear advection term, (c) surface drag baroclinic component, and (d) vertical advection term, stippled as in Fig. 5. See text for a description of each term.

seen in the temperature anomalies of Fig. 1c, and encounters the regions of strong climatological shear in the subtropics.

5. Conclusions

We have investigated the mechanisms that generate the SLP anomalies in the western Pacific, which have long been known as part of the classic Southern Oscillation pattern associated with ENSO. Contrary to the traditional view that assumes a single deep baroclinic mode for ENSO response in the tropics, the SLP anomalies in the western Pacific occur in a region where there is little baroclinic signal associated with the tropospheric temperature anomalies in NCEP–NCAR reanalysis, CMIP5 models, and QTCM. Separation of the SLP into its baroclinic and barotropic components indicates that the baroclinic mode SLP contributions extend over the central and eastern equatorial Pacific, coincident with the temperature anomalies, and in a spatial pattern consistent with first baroclinic mode

wave dynamics. On the other hand, SLP anomalies in the western Pacific arise primarily from barotropic mode contributions and thus must be associated with a slightly more complex dynamical pathway.

The following pathway is found in QTCM diagnostic experiments: interactions with SST anomalies create the baroclinic mode signal in the central and eastern Pacific, but baroclinic–barotropic interactions, arising substantially in the subtropical Pacific, create a barotropic response. This barotropic contribution is widespread in the tropics, but it is particularly important in yielding the SLP anomaly pattern in the western Pacific where the baroclinic contribution is small. In a set of QTCM experiments, we suppress anomalies in baroclinic–barotropic interaction terms over increasingly wider latitudinal bands in the tropical Pacific, to diagnose their effects on the SLP anomalies in the western Pacific associated with ENSO. In the 15°N – 15°S experiment, the pressure signals in the western Pacific are only partly suppressed, whereas in the 30°N – 30°S suppression experiment, the anomalies in the western Pacific are

almost entirely removed. We note that the suppression experiment does not necessarily imply that the westward teleconnection is purely barotropic. However, it does demonstrate that anomalies of an effective barotropic Rossby wave source due to the baroclinic–barotropic interaction terms are key to maintaining the largely barotropic signal in the western Pacific that yields the classical SLP patterns in this region. Furthermore, it demonstrates the importance of the subtropical contribution to this effective Rossby wave source. This arises substantially from the vertical shear term that occurs as the ENSO baroclinic anomalies, spread by wave dynamics into the subtropics, interact with basic-state vertical shear approaching the subtropical jet.

Acknowledgments. We thank Joyce Meyerson for her assistance with graphics. This work was supported in part by National Science Foundation Grants AGS-1102838 and AGS-1041477, National Oceanic and Atmospheric Administration Grants NA11OAR4310099 and NA14OAR4310274, and a scholarship awarded by the Chinese Scholarship Council to support XJ's doctoral study at the University of California, Los Angeles. We thank Hui Su and Matt Munnich for their unpublished initial QTCM and NCEP analysis (2004) related to this problem. We also thank Xin Qu for his comments. JDN would like to acknowledge the role of Plate 8 from Wallace et al. (1998) in which the mismatch of SLP and tropospheric temperature patterns led to the puzzle analyzed here.

REFERENCES

- Bacmeister, J. T., and M. J. Suarez, 2002: Wind stress simulations and the equatorial momentum budget in an AGCM. *J. Atmos. Sci.*, **59**, 3051–3073, doi:10.1175/1520-0469(2002)059<3051:WSSATE>2.0.CO;2.
- Berlage, H. P., 1957: Fluctuations of the general atmospheric circulation of more than one year, their nature and prognostic value. Koninkijk Nedeerlands Meteorologisch Instituut Mededelingen en Verhandelingen 69, 152 pp.
- Biello, J. A., and A. J. Majda, 2004a: Boundary layer dissipation and the nonlinear interaction of equatorial baroclinic and barotropic Rossby waves. *Geophys. Astrophys. Fluid Dyn.*, **98**, 85–127, doi:10.1080/03091920410001686712.
- , and —, 2004b: The effect of meridional and vertical shear on the interaction of equatorial baroclinic and barotropic Rossby waves. *Stud. Appl. Math.*, **112**, 341–390, doi:10.1111/j.0022-2526.2004.01518.x.
- Branstator, G., 1983: Horizontal energy propagation in a barotropic atmosphere with meridional and zonal structure. *J. Atmos. Sci.*, **40**, 1689–1708, doi:10.1175/1520-0469(1983)040<1689:HEPIAB>2.0.CO;2.
- Chiang, J. C. H., and A. H. Sobel, 2002: Tropical tropospheric temperature variations caused by ENSO and their influence on the remote tropical climate. *J. Climate*, **15**, 2616–2631, doi:10.1175/1520-0442(2002)015<2616:TTVCB>2.0.CO;2.
- Gill, A. E., 1980: Some simple solutions for heat-induced tropical circulation. *Quart. J. Roy. Meteor. Soc.*, **106**, 447–462, doi:10.1002/qj.49710644905.
- Held, I. M., and I. S. Kang, 1987: Barotropic models of the extratropical response to El Niño. *J. Atmos. Sci.*, **44**, 3576–3586, doi:10.1175/1520-0469(1987)044<3576:BMOTER>2.0.CO;2.
- , R. L. Panetta, and R. T. Pierrehumbert, 1985: Stationary external Rossby waves in vertical shear. *J. Atmos. Sci.*, **42**, 865–883, doi:10.1175/1520-0469(1985)042<0865:SERWIV>2.0.CO;2.
- Horel, J. D., and J. M. Wallace, 1981: Planetary-scale atmospheric phenomena associated with the Southern Oscillation. *Mon. Wea. Rev.*, **109**, 813–829, doi:10.1175/1520-0493(1981)109<0813:PSAPAW>2.0.CO;2.
- Hoskins, B. J., and D. J. Karoly, 1981: The steady linear response of a spherical atmosphere to thermal and orographic forcing. *J. Atmos. Sci.*, **38**, 1179–1196, doi:10.1175/1520-0469(1981)038<1179:TSLROA>2.0.CO;2.
- Ji, X., J. D. Neelin, S. K. Lee, and C. R. Mechoso, 2014: Interhemispheric teleconnections from tropical heat sources in intermediate and simple models. *J. Climate*, **27**, 684–697, doi:10.1175/JCLI-D-13-00017.1.
- Kalnay, E., and Coauthors, 1996: The NCEP/NCAR 40-Year Reanalysis Project. *Bull. Amer. Meteor. Soc.*, **77**, 437–471, doi:10.1175/1520-0477(1996)077<0437:TNYRP>2.0.CO;2.
- Kiladis, G. N., and H. F. Diaz, 1989: Global climatic anomalies associated with extremes in the Southern Oscillation. *J. Climate*, **2**, 1069–1090, doi:10.1175/1520-0442(1989)002<1069:GCAAWE>2.0.CO;2.
- Kumar, A., and M. P. Hoerling, 2003: The nature and causes for the delayed atmospheric response to El Niño. *J. Climate*, **16**, 1391–1403, doi:10.1175/1520-0442-16.9.1391.
- Lee, S. K., C. Z. Wang, and B. E. Mapes, 2009: A simple atmospheric model of the local and teleconnection responses to tropical heating anomalies. *J. Climate*, **22**, 272–284, doi:10.1175/2008JCLI2303.1.
- Lintner, B. R., and J. C. H. Chiang, 2007: Adjustment of the remote tropical climate to El Niño conditions. *J. Climate*, **20**, 2544–2557, doi:10.1175/JCLI4138.1.
- Majda, A. J., and J. A. Biello, 2003: The nonlinear interaction of barotropic and equatorial baroclinic Rossby waves. *J. Atmos. Sci.*, **60**, 1809–1821, doi:10.1175/1520-0469(2003)060<1809:TNI0BA>2.0.CO;2.
- Matsuno, T., 1966: Quasi-geostrophic motions in the equatorial area. *J. Meteor. Soc. Japan*, **44**, 25–43.
- Neelin, J. D., and N. Zeng, 2000: A quasi-equilibrium tropical circulation model—Formulation. *J. Atmos. Sci.*, **57**, 1741–1766, doi:10.1175/1520-0469(2000)057<1741:AQETCM>2.0.CO;2.
- , and H. Su, 2005: Moist teleconnection mechanisms for the tropical South American and Atlantic sector. *J. Climate*, **18**, 3928–3950, doi:10.1175/JCLI3517.1.
- Sardeshmukh, P. D., and B. J. Hoskins, 1988: The generation of global rotational flow by steady idealized tropical divergence. *J. Atmos. Sci.*, **45**, 1228–1251, doi:10.1175/1520-0469(1988)045<1228:TGOGRF>2.0.CO;2.
- Simmons, A. J., 1982: The forcing of stationary wave motion by tropical diabatic heating. *Quart. J. Roy. Meteor. Soc.*, **108**, 503–534, doi:10.1002/qj.49710845703.
- , J. M. Wallace, and G. W. Branstator, 1983: Barotropic wave propagation and instability, and atmospheric teleconnection patterns. *J. Atmos. Sci.*, **40**, 1363–1392, doi:10.1175/1520-0469(1983)040<1363:BWPAlA>2.0.CO;2.
- Su, H., and J. D. Neelin, 2002: Teleconnection mechanisms for tropical Pacific descent anomalies during El Niño. *J. Atmos.*

- Sci.*, **59**, 2694–2712, doi:10.1175/1520-0469(2002)059<2694:TMFTPD>2.0.CO;2.
- , —, and C. Chou, 2001: Tropical teleconnection and local response to SST anomalies during the 1997–1998 El Niño. *J. Geophys. Res.*, **106**, 20 025–20 043, doi:10.1029/2000JD000124.
- , —, and J. E. Meyerson, 2003: Sensitivity of tropical tropospheric temperature to sea surface temperature forcing. *J. Climate*, **16**, 1283–1301, doi:10.1175/1520-0442-16.9.1283.
- , —, and —, 2005: Mechanisms for lagged atmospheric response to ENSO SST forcing. *J. Climate*, **18**, 4195–4215, doi:10.1175/JCLI3514.1.
- Taylor, K. E., R. J. Stouffer, and G. A. Meehl, 2012: An overview of CMIP5 and the experiment design. *Bull. Amer. Meteor. Soc.*, **93**, 485–498, doi:10.1175/BAMS-D-11-00094.1.
- Trenberth, K. E., 1997: The definition of El Niño. *Bull. Amer. Meteor. Soc.*, **78**, 2771–2777, doi:10.1175/1520-0477(1997)078<2771:TDOENO>2.0.CO;2.
- Walker, G. T., 1923: Correlation in seasonal variations of weather VIII. *Mem. India Meteor. Dept.*, **24**, 75–131.
- Wallace, J. M., E. M. Rasmusson, T. P. Mitchell, V. E. Kousky, E. S. Sarachik, and H. von Storch, 1998: The structure and evolution of ENSO-related climate variability in the tropical Pacific: Lessons from TOGA. *J. Geophys. Res.*, **103**, 14 241–14 259, doi:10.1029/97JC02905.
- Wang, B., and X. S. Xie, 1996: Low-frequency equatorial waves in vertically sheared zonal flow. Part I: Stable waves. *J. Atmos. Sci.*, **53**, 449–467, doi:10.1175/1520-0469(1996)053<0449:LFEWIV>2.0.CO;2.
- Webster, P. J., 1972: Response of tropical atmosphere to local, steady forcing. *Mon. Wea. Rev.*, **100**, 518–541, doi:10.1175/1520-0493(1972)100<0518:ROTTAT>2.3.CO;2.
- Zeng, N., J. D. Neelin, and C. Chou, 2000: A quasi-equilibrium tropical circulation model—Implementation and simulation. *J. Atmos. Sci.*, **57**, 1767–1796, doi:10.1175/1520-0469(2000)057<1767:AQETCM>2.0.CO;2.